IMPACT: International Journal of Research in Engineering and Technology
ISSN (P): 2347–4599; ISSN (E): 2321–8843
Vol. 10, Issue 4, Apr 2022, 11–34

AGE AND TECTONIC SETTING OF TUANJIEDABAN INTERMEDIATE ACID INTRUSIVE ROCKS IN WESTERN QIANGTANG BASIN, TIBET

Zhao Shouren[1], Chen Haixia[2], Chen Lingkang[3] & Zhu Leyi[4]

[1]Research Scholar, Regional Geological Surveying Party, Tibet Bureau of Geology and Exploration and Exploitation of Mineral Resources, Lhasa 851400, China

[2]Research Scholar, College of Petroleum Engineering, Guangdong University of Petrochemical Technology, Maoming 525000, China

[3,4]Research Scholar, College of Sciences, Guangdong University of Petrochemical Technology, Maoming 525000, China

Received: 17 Apr 2022 **Accepted:** 23 Apr 2022 **Published:** 27 Apr 2022

ABSTRACT

There is great controversy with the closure time of Bangong Lake-Nujiang Tethys Oceanfor a long time. A detailed petrological, geochemical and zircon U-Pb dating of the Tuanjiedaban intermediate acid intrusive rocks in Western Qiangtang Basin have been undertaken in this paper. The results show that the samples of the Tuanjiedaban intermediate acid intrusive rocks are characterized by high silicon (SiO_2 is 57.56% -72.35%), rich alkali (K_2O + Na_2O contents of 5.43% -10.41%), and peraluminous (A / CNK values of 1.0-1.51). The intrusive belongs to high potassium calc alkaline I-type granite. The trace elements of samples are enriched in Rb, Th, U, K and other large ion lithophile elements, but relatively depleted in Nb, Ta, Ti, and other high field strength elements. Light rare earth is enriched, and there is a weak negative Eu anomaly （δEU is 0.15-0.45), indicating that due to the subduction collision island arc tectonic environment, the subsidence of the ocean crust lithosphere triggered the underplating of mantle derived magma, accompanied by the melting of part of the crust. Zircon U-Pb dating results show that their formation ages are 120.33±0.99 Ma, 122.5±2.0 Ma and 125.7±2.1 Ma respectively, belonging to the middle and late Early Cretaceous, which is basically consistent with the formation time of Dongcuo, Zhongcang and duolong rocks on Bangong Lake Nujiang magmatic arc belt, and they are the products of Bangong Lake Nujiang Tethys ocean subduction collision. This study provides new constraints for understanding the tectono magmatic evolution of Bangong Lake Nujiang junction zone.

KEYWORDS: *Zircon U-Pb Age Tectonic Environment Tuandaban Rock Mass Bangonghu Nujiang Junction Zone*

INTRODUCTION

The Qiangtang Basin located in the northern part of the Bangonghu Nujiang junction zone, which is associated with the subduction-closure of the Paleo-New Tethys Ocean tectonic belt. It has experienced complex tectonic events (Huang, 2001). In the early and middle Jurassic, the Bangonghu Nujiang Tethys Ocean began to rift and form oceanic volcanic arc basalt in 220-189 Ma, indicating the basin expansion ridge environment (Wu et al., 2018). The stable marine strata indicates that the Bangong Lake-Nujiang Ocean Basin in the Middle Jurassic became stable from activity (Song et al., 2019), which is widely distributed in the combination zone and on both sides of the Renduo Formation, Mali Formation, Sangalamian Formation, as well as the Shaqiaomu Formation in South Qiangtang and Jiebuqu Formation in the Middle

Jurassic. In the middle and late Jurassic, the Bangong Lake-Nujiang Tethys Ocean began to subduct (Zeng et al., 2018). From the late Jurassic to the early Cretaceous, it evolved into the residual basin represented by the limestone of the Tukari Formation and developed the Zap-Dobuza magmatic arc and the Anglonggangri-Bango magmatic arc on the south side (Geng et al., 2015). The formation of the magmatic arc recorded the process of subduction, melting and upwelling of the oceanic crust on the edge of the continental plate (Li et al., 2014). In recent years, a number of mafic-moderately acidic magmatic rocks have been found in Dongcuo (Che et al., 2021) in the south of Qiangtang, Dugur area in the north of Gize County (Liu et al., 2018), Xiabiecuo (Wang et al., 2021) in the north of Nima, Maierze (Fan et al., 2016), Zhongcang (Fan et al., 2014), and Duolong (Li et al., 2016), and their zircon ages are between 127 and 100 Ma, indicating that the Bangong Lake-Nujiang Ocean subducts southward and northward. As a result, a wedge-shaped accretionary body (Li et al., 2011) was formed in the southern margin of the South Qiangtang Block. A large number of intermediate-acid magmatic activities formed the tectonic-magmatic arc in the western section of the Bangonghu Nujiang (Zhu et al., 2015).

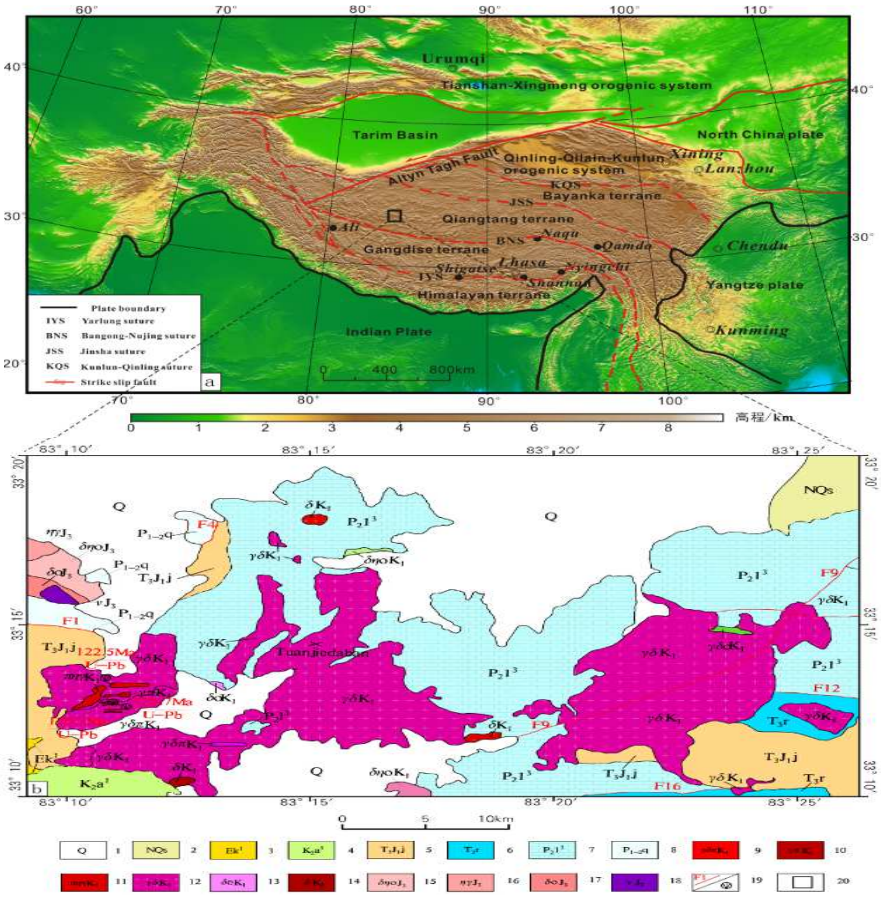

1. Loose deposits with silt, sand and gravel; 2. Suonahu formation: conglomerate mixed with limestone and gypsum salt; 3. First segment of Kangtuo formation: conglomerate, pebbly sandstone; 4. First segment of Abushan formation: multicomponent conglomerate and calcareous fine sandstone; 5. Jiburia formation:calcareous slate and limestone; 6. Riganpeicuo formation: arenaceous limestone mixed with micrite limestone; 7. Third of Longgeformaton: micrite limestone, bioclastic limestone; 8. Qudi formation:quartzite, slate, phyllite and sandstone; 9. Gray White Granodiorite Porphyry; 10. light skin red granite porphyry; 11. porphyritic monzogranite; 12. biotite hornblende granodiorite; 13. quartz diorite; 14. fine grained diorite; 15. quartz monzodiorite; 16. monzogranite; 17. quartz diorite; 18. gabbro; 19. fault / zircon sampling point; 20. location of study area

Figure 1: Location and Regional Geological Map of the Study Area, Location of Study Area (a. Modified after Duan et al.,2020) and Regional Geological Map, (b. Modified after Zhao et l., 2015).

The survey of 1: 50 000 Maierze and other five regional geological (Zhao et al., 2015) show that granodiorite, monzogranite and other neutral-acid deep-seated intrusive rocks are widely distributed in the Tuanjiedaban area of southern Qiangtang. In addition, there are vein-like occurrences of shallow-formed granite porphyry, granodiorite porphyry and other intrusive bodies (Fig1).In recent years, an important Duolong ore concentration area in the BangonghuNujiang metallogenic belt has been found in the southeast of the study area (Li et al., 2013 ; Sun, et al., 2017 ; li et al., 2016). The porphyry Cu-Au deposit was found in Qingcaoshan area outside the Duolong ore concentration area (Zheng et al., 2018). Its ore-bearing granodiorite porphyry and granodiorite were formed between 118 Ma and 130 Ma, with typical island arc magmatic characteristics (Zhou et al., 2013; Zheng et al., 2018).The above studies have greatly improved the research heat on the metallogenic geological background of porphyry deposits in the South Qiangtang Basin. Do the granite diorite porphyry, granite porphyry and other rock bodies exposed in the Tuanjiedaban area have similar metallogenic geological background with many other places? In this paper, on the basis of regional investigation, the petrological and geochemical characteristics of intermediate-acid magmatic rocks in Tuanjiedaban area are studied in detail. The samples are collected for zircon U-Pb isotope dating. The tectonic environment of the rock mass in the region is discussed, which provides age basis for the study of metallogenic geological background in the region.

REGIONAL GEOLOGY

The study area is located in the northwest of Gaize County in Tibet. The tectonic position belongs to the Qiangtang block (Fig. 1). The Paleozoic Permian Qudi Formation ($P_{1\text{-}2}q$) in the area is composed of fine sandstone, quartz sandstone, quartz siltstone and calcareous slate in feldspar quartz, which is generally shallow shelf sedimentary environment. The lithology of the Jilongge Formation (P_2l) is mainly dark gray medium-thick layered micrite bioclastic limestone and micrite limestone. It has fault contact with underlying strata Qudi formation. The Upper Triassic Rigan Diaocuo Formation (T_3r) of the Mesozoic Erathem is composed of light gray-gray medium-to-thick layered sandy lithic limestone with microcrystalline limestone, which is in fault contact with the underlying Longge Formation and in integrated contact with the upper Jurassic Jipuriya Formation. Jurassic Jipuri a Formation (T_3J_1j) is composed of dark gray calcareous sandstone and silty slate interbedded with limestone and conglomerate. The above sedimentary assemblages reflect the passive continental margin environment. The rocks suffer from unbalanced regional metamorphism. The passive continental compression environment characteristics are real in many places in the South Qiangtang Basin (Zhao et al., 2015; Liang et al., 2017). The Cretaceous Abushan Formation (K_2a) is a combination of purple-red, dark-red medium-thick layered coarse sandstone and fine sandstone, with gray-white gypsum salt layer locally. The upper part is brown-red sandstone interbedded with gray-white medium-thin calcareous siltstone. The sedimentary environment is the red molasses formation in the intermountain basin, which has angular unconformity contact with the underlying strata, and then is covered by the Kangtuo Formation angular unconformity. Paleogene Kangtuo Formation (E*k*) is the red molasses assemblage in the intermountain basin. Neogene Suonahu Formation (NQ*s*) is a carbonate-clastic rock association. Quaternary is loose accumulation of intermountain basin (Zhao et al., 2015).

The magmatic rocks in the area are mainly intermediate-acid intrusive bodies in Cretaceous, mainly produced by stock, dike and etc. Lithology has acid granite porphyry, monzonitic granite porphyry, granodiorite porphyry and other shallow facies. The lithology of the plutonic intrusions are porphyritic monzogranite, granodiorite, monzogranite and diorite (Zhao et al., 2015). Its spatial distribution is shown in Fig 1.

Near east-west fault structure constitutes the main structural pattern of the survey area, which is the first stage of fault structure in the survey area. According to the cutting relationship between geological bodies, its formation age is about Late Jurassic. NE-trending and NW-trending faults are mainly characterized by reverse faults and translational faults, forming later than EW-trending faults about the late Late Cretaceous. The north-south fault is not developed, which has tensile characteristics. The formation age is relatively late (Zhao et al., 2015).

SAMPLE COLLECTION AND ANALYSIS

In this paper, a total of 45 rock slice samples, 11 silicates, rare earths and major or trace elements, and 3 zircon samples were collected from rock masses with different lithology such as Tuanjiedaban granodiorite, granite porphyry and granodiorite porphyry.

Rock slice samples are completed by Xi ' an Mineral Resources Supervision and Testing Center of Ministry of Land and Resources. The analysis of silicate, rare earth and major trace elements was completed by Southwest Geological and Metallurgy Test. Silicate analysis using lithium metaborate melting, followed by X-ray fluorescence spectrometry (XRF). The detection limit is 0.01-100 %. The specific analysis method is shown in the literature (Luo et al., 2008). Rare earth and trace elements were melted with lithium metaborate and then quantitatively analyzed by plasma mass spectrometer. The detection limit was 0.01-1000 ppm. The test steps are shown in the literature (Shi, 2013).

LA-ICP-MS zircon U-Pb dating samples were sorted by heavy liquid and magnetic methods in the laboratory of Hebei Provincial Institute of Regional Geological Survey. Target preparation and cathode luminescence (CL) images were completed in the Institute of Geology in Chinese Academy of Geological Sciences. In situ U-Th-Pb isotopic analysis of zircons by transmission and reflection light and laser plasma mass spectrometer (LA-ICP-MS) was performed at the State Key Laboratory of Geological Processes and Mineral Resources in China University of Geosciences (Wuhan). The laser ablation system is GeoLas 2005 and the ICP-MS is Agilent 7500a. Zircon ages are calculated using international standard zirconium 91500 as the external standard, and according to Andersen (2002) methodis corrected . Age calculation and harmonic diagram drawing are mainly completed by Isoplot program. The detailed analysis process is shown in the literature (Liu et al., 2010; Wang et al., 2017 ,liu et al., 2018).

RESULT AND DISCUSSION

Petrological Characteristics

In this study, the main lithology of rock mass collected in Tuanjiedaban is granodiorite, quartz monzodiorite, monzogranite, diorite, porphyritic monzogranite, dolomite diorite, granodiorite porphyry and granite porphyry (Zhao et al., 2015). Among them, the granite diorite have the largest distribution area (Fig. 1b)which is mainly exposed in Tuanjiedaban and its periphery. The fine-grained diorite (δK_1) is mostly distributed in the edge of coarse and medium-grained biotite hornblende granodiorite ($\gamma\delta K_1$). There is a gradual influx-intrusive contact relationship between them. Fine-grained monzogranite ($\eta\gamma K_1$) and light-grey medium-fine-grained quartz diorite ($\delta o K_1$) are mostly distributed as small rock beads, which are intruded into the Permian Longge Formation and have pulsating intrusive contact with coarse-medium-grained biotite hornblende granodiorite ($\gamma\delta K_1$).The hypabyssal intrusive rocks are mainly including granite porphyry ($\gamma\pi K_1$), monzogranite porphyry ($\eta\gamma\pi K_1$) and granodiorite porphyry ($\gamma\delta\pi K_1$). There are various types of porphyry are mostly vein-like intrusive granite diorite rocks. This paper select two types of characteristic lithology as follows:

The rock is gray-white, coarse and medium-grained granite and block structure of Coarse and medium-grained biotite hornblende diorite ($\gamma\delta$K1) (Fig2). The rocks are mainly composed of plagioclase, quartz, potassium feldspar, hornblende, biotite, epidote, apatite, zircon, sphene and metal minerals. Quartz, plagioclase, potash feldspar, hornblende and other dark minerals respectly accounts for about 28 %, 43 %, 15 % and 13 % of the total mineral. The secondary mineral has much sphene, followed by apatite.

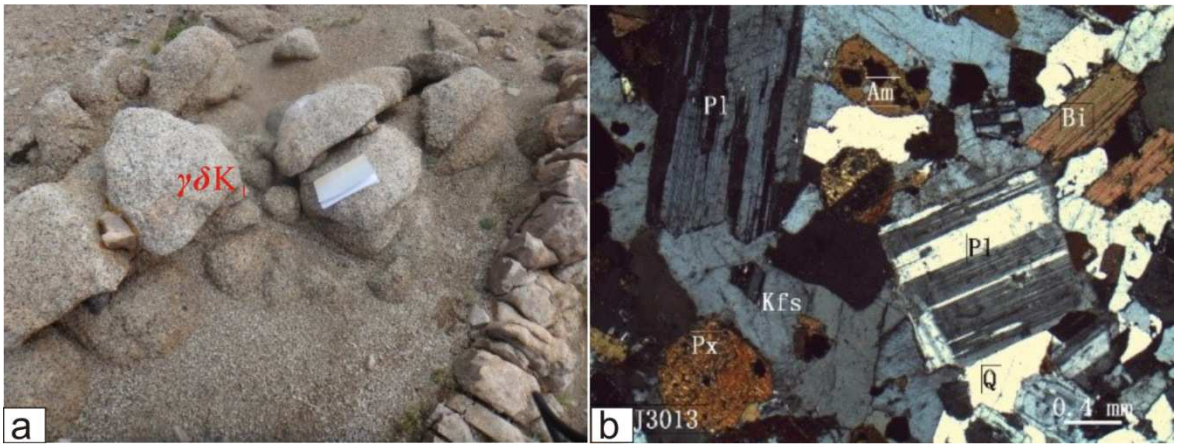

Figure 2: Field Photographs(a) and Microphotographs of the Coarse Medium Grained Biotite Hornblende Granodiorite(b) (Q- quartz; Pl- plagioclase; Kfs- Potassium feldspar; Am- Amphibole; Bi- Biotite; Px- pyroxene)

The plagioclase is mostly semi-automorphic lath-like (Fig.2b). Most of which have particle sizes of 1.03 mm×2.00mm-2.57 mm×3.72mm. Some have length and diameter less than 2.00 mm, but less than 20 % of the total plagioclase. Potash feldspar is partly slate-column and partly heteromorphic (Fig.2b) .The particle size is generally larger than that of plagioclase. The phenomenon of wrapping that plagioclase is wrapped or partially wrapped. A small number of Cass double crystals are visible, which are orthoclase. Quartz is its crystal. The general particle size is 2.00mm-5.00mm. Some are less than 2.00mm or greater than 5.00mm. The maximum particle size is 8.00mm. The amphibole is mostly columnar. Some are irregular (Fig.2b). Most of the columns are about 2.00 mm×5.00 mm. A few are reached to 3.00 mm×7.00 mm.

Granodiorite porphyry ($\gamma\delta\pi K_1$): Field investigation shows that the rock is strongly weathered. The surface outcrop is broken (Fig.3a). The rock is grayish-white, patchy structure, massive structure, and the matrix has micro-crystalline structure. The rock is composed of phenocryst and matrix. The phenocryst accounts for about 38 % of the total volume of the rock and the matrix accounts for about 62 % (Fig.3b). The main characteristics of the rock are that the matrix has a micro-crystalline structure and the alteration, especially strong sericitization. The phenocrysts are mainly plagioclase, followed by quartz, potash feldspar, chlorite biotite and amphibole. Quartz is about 21 % of the total phenocrysts. Plagioclase is about 87 % of the total plagioclase. Black mica, hornblende have been chloritization. It can see a small number of visible residual crystal. Matrix is mainly composed of feldspar, quartz, sericite, calcite, chlorite and etc. Accessory minerals are titanite and zircon.

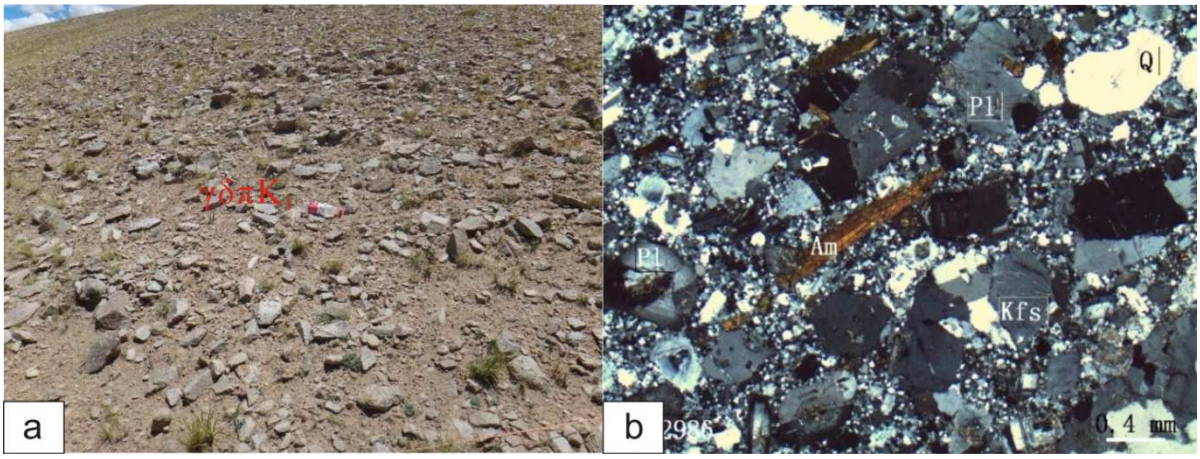

Figure 3: Field Photographs(a) and Microphotographs of the Granodiorite Porphyry(b) (Q-quartz; Kfs-Potassiumfeldspar; Pl-plagioclase; Am- Amphibole).

Geochemical Characteristics of Rocks

Major Element Analyses

The petrochemistry constant components of intrusive rocks in the study area are shown in Table 1. Its CIPW standard minerals and main parameters are shown in Table 2. The average SiO_2

Table 1: Analytical Results of Major Elements of Early Cretaceous Intrusive Rocks

Sample No.	Rock name	SiO_2	Al_2O_3	Fe_2O_3	FeO	CaO	MgO	K_2O	Na_2O	TiO_2	P_2O_5	MnO	LOI	H_2O^-	CO_2
		10^{-2}	10^{-2}	10^{-2}	10^{-2}	10^{-2}	10^{-2}	10^{-2}	10^{-2}	10^{-2}	10^{-2}	10^{-2}	10^{-2}	10^{-2}	10^{-2}
PM002-1GS2	quartz diorite	63.50	15.78	2.40	2.56	5.14	2.01	3.22	2.80	0.529	0.143	0.105	1.27	0.122	0.187
PM002-1GS3	hornblende granodiorite	63.90	15.82	2.40	2.53	5.00	2.05	3.04	2.90	0.528	0.140	0.116	1.23	0.298	0.191
PM002-2GSI	monzogranite	72.01	14.45	1.19	0.790	2.22	0.562	4.60	3.00	0.222	0.068	0.054	0.810	0.314	0.119
PM002-4GS1	granite porphyry	72.35	13.49	0.260	0.490	1.58	0.622	7.05	2.00	0.227	0.119	0.019	1.44	0.358	0.345
PM003-2GS2	granite porphyrygranite porphyry	66.79	15.21	2.03	1.82	3.63	1.46	4.07	2.94	0.438	0.118	0.085	1.07	0.410	0.454
PM003-5GS1	tonalite	62.74	15.86	2.72	2.56	5.48	2.27	2.99	2.93	0.522	0.146	0.116	1.30	0.302	0.390
ED306-GS1	diorite	58.82	16.83	0.350	1.82	6.42	2.93	8.29	2.12	0.478	0.142	0.068	1.59	0.286	0.573
ED312-GS1	quartz diorite	63.82	15.56	2.33	2.05	5.94	2.14	2.88	2.96	0.513	0.139	0.057	1.25	0.325	0.233
ED315-GS1	quartz monzodiorite	64.61	16.44	1.22	2.48	4.66	1.52	3.19	3.15	0.417	0.105	0.054	1.77	0.557	0.223
GD313-GS1	Amphibole monzodiorite	63.36	16.10	3.01	2.29	4.95	1.81	2.88	2.82	0.675	0.191	0.100	1.39	0.347	0.138
HD229-GS1	Hornblende granodiorite	57.56	16.03	2.84	4.32	6.14	2.83	2.69	2.74	0.72	0.19	0.16	3.19	0.29	0.39
Average		64.50	15.56	1.887	2.1554	4.650	1.8	4.081	2.76	0.479	0.136	0.085	1.482	0.328	0.295

Table 2: CIPW Standard Mineral Calculation and Characteristic Parameters of Early Cretaceous Intrusive Rocks

Sample No.	CIPW Standard Mineral Content (wt%)														Characteristic Parameter				
	Q	C	Or	Ab	An	Di(FS)	Di(MS)	Hy(MS)	Hy(FS)	Ol(MS)	Ol(FS)	Mt	Il	Ap	DI	AR	SI	δ	A/CNK
PM002-1GS2	21.52	0.00	19.738	24.133	21.364	0.771	2.171	4.092	1.667	0.00	0.00	3.544	1.024	0.338	65.031	0.188	15.402	1.768	0.90
PM002-1GS3	22.042	0.00	18.255	24.928	21.509	0.568	1.657	4.42	1.739	0.00	0.00	3.535	1.018	0.329	65.225	1.798	15.867	1.688	0.92
PM002-2GSI	31.726	0.668	27.415	25.597	10.657	0.00	0.00	1.412	0.203	0.00	0.00	1.74	0.426	0.16	84.738	2.262	5.541	1.991	1.03
PM002-4GS1	30.15	0.00	42.425	17.236	7.133	0.008	0.039	1.558	0.347	0.00	0.00	0.384	0.439	0.28	89.811	4.0007	5.968	2.791	0.98
PM003-2GS2	24.543	0.00	24.295	25.233	16.516	0.161	0.612	3.405	1.03	0.00	0.00	2.985	0.843	0.278	73.171	2.185	11.850	2.066	0.96
PM003-5GS1	20.115	0.00	17.971	25.216	21.651	0.877	3.15	4.289	1.37	0.00	0.00	4.01	1.009	0.343	63.302	1.768	16.852	1.775	0.88
ED306-GS1	0.055	0.00	49.845	18.252	12.134	3.438	12.044	1.844	0.604	0.00	0.00	0.516	0.923	0.336	68.161	2.621	18.891	6.850	0.70
ED312-GS1	21.609	0.00	17.297	25.453	21.005	0.971	5.398	2.915	0.601	0.00	0.00	3.433	0.99	0.327	64.359	1.746	17.313	1.638	0.83
ED315-GS1	21.486	0.00	19.265	27.238	21.768	0.387	0.568	3.605	2.818	0.00	0.00	1.808	0.809	0.248	67.989	1.859	13.149	1.860	0.96
GD313-GS1	23.353	0.00	17.333	24.302	23.186	0.058	0.377	4.416	0.773	0.00	0.00	4.445	1.305	0.452	64.988	1.743	14.130	1.596	0.96
HD229-GS1	14.116	0.00	16.523	24.099	24.416	1.786	3.076	5.90	3.93	0.00	0.00	4.28	1.421	0.456	54.738	1.649	18.353	2.025	0.86
Average	20.974	0.67	24.578	23.790	18.304	0.820	2.645	3.441	1.371	0.00	0.00	2.79	0.928	0.290	69.228	1.983	13.938	2.368	0.89

Content of intrusive rocks is 64.50 %. The total alkali content $K_2O + Na_2O$ is 6.84 %. The average K_2O / Na_2O is 1.48. The contents of FeO (2.16 %), MgO (1.84 %) and CaO (4.65 %) are slightly higher. The content of Al_2O_3 (15.60 %) is also higher. The content of P_2O_5 (0.14 %) is within the range of typical island arc magma (< 0.25 %). Quartz Q appears in standard minerals and corundum molecule C is rare. The CIPW standard mineral assemblage is Q + An + Ab + Or + Di + Hy. The average differentiation index DI is 69.23. The average consolidation index is 13.94, indicating that the degree of crystallization differentiation of magma is high. The average alkalinity AR is 1.93. A / CNK is more than 1.1, varying from 1.2 to 1.51, which is metaaluminous with an average of 1.38. The Ritman index δ is 2.37, belonging to the Pacific calc-alkaline rock series. In the SiO_2 - K_2O diagram of rock mass (Fig.4), the vast majority of samples fall into the high-K calc-alkaline rock series. In the A-F-M diagram of granite (Fig.5), all samples fall into the high-K calc-alkaline series, which is consistent with the rock series reflected by the Reitman index. They are all calc-alkaline series rocks.

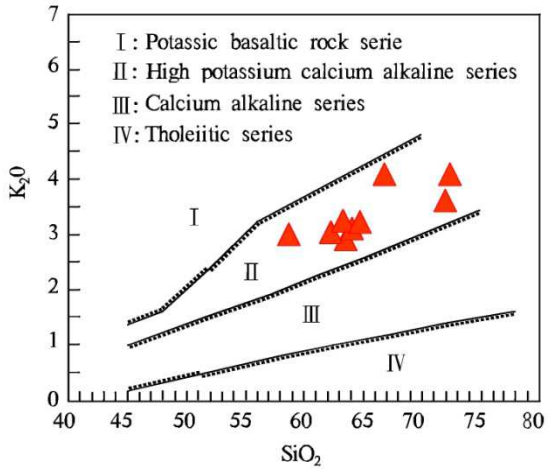

Figure 4: Diagrams of SiO_2-K_2O for Intrusive Rocks in the Study Area (from Peccerillo et al.,1976).

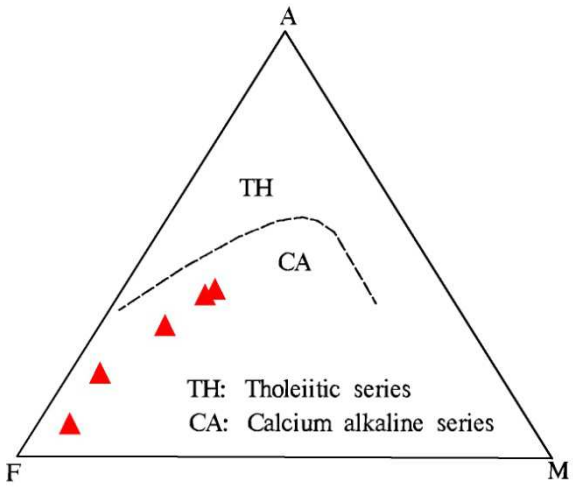

Figure 5: Diagrams of A-F-M for Intrusive Rocks in the Study Area (from Papu and Philip,1989).

Rock Characteristics of Trace and Rare Earth Elements

The abundance of rare earth elements and trace elements in the early Cretaceous intrusive rocks in the survey area can be respectively seen in Table 3 and Table 4. The rare earth element content of intrusive rocks is medium with an average total ΣREE of 152.56×10^{-6}. LREE / HREE is average of 3.15. It indicates that the light rare earth has a high fractionation degree. δ Eu is average of 0.28. It has weak negative Eu anomaly, suggesting that the source region has a high degree of separation and crystallization or plagioclase remains in the source region during partial melting (Tepper et al., 1993).

Table 3: Analytical Results of REE of Samples from the Early Cretaceous Intrusive Rocks

Sample No.	Rare Earth Element Content (10^{-6})															Characteristic parameter		
	La	Ce	Pr	Nd	Sm	Tb	Gd	Eu	Dy	Ho	Er	Tm	Yb	Lu	Y	ΣREE	LREE/HREE	δ Eu
PM002-1XT2	28.2	47.0	6.45	20.5	3.87	0.64	3.69	1.13	3.94	0.82	2.53	0.44	2.81	0.43	23.4	146.93	2.70	0.299
PM002-1XT3	34.2	67.1	6.58	20.9	3.78	0.64	3.66	1.14	3.90	0.82	2.46	0.44	2.86	0.41	21.0	170.8	3.60	0.306
PM002-2XTI	29.0	58.5	5.32	15.4	2.51	0.38	2.52	0.81	2.17	0.45	1.36	0.23	1.63	0.24	13.5	136.29	4.51	0.322
PM002-4XT1	25.2	43.6	4.77	14.0	2.38	0.33	2.25	1.06	1.79	0.35	1.04	0.18	1.31	0.18	10.4	110.24	4.73	0.458
PM003-2XT2	41.8	96.6	9.17	26.4	4.38	0.65	4.23	0.74	4.16	0.83	2.63	0.48	3.45	0.51	23.8	221.95	4.18	0.168
PM003-5XT1	27.7	56.0	5.78	18.8	3.44	0.58	3.31	1.01	3.50	0.71	2.19	0.36	2.35	0.34	20.2	147.32	3.26	0.299
ED306-XT1	22.8	44.2	5.96	19.4	3.70	0.61	3.57	1.25	3.78	0.77	2.35	0.41	2.72	0.41	19.7	135.92	2.52	0.344
ED312-XT1	26.8	46.3	5.91	19.8	3.86	0.65	3.63	1.13	4.01	0.82	2.46	0.44	2.78	0.42	21.1	141.47	2.76	0.302
ED315-XT1	22.4	44.2	5.34	17.4	3.28	0.55	3.25	1.05	3.25	0.66	3.37	0.34	2.25	0.33	17.8	126.17	2.88	0.324
GD313-XT1	31.3	67.2	7.38	24.6	4.75	0.80	4.61	1.35	4.61	1.01	4.92	0.50	3.18	0.48	25.6	182.09	3.00	0.171
HD229-XT1	30.7	56.9	6.25	25.5	4.54	0.70	4.70	1.25	4.70	0.77	3.67	0.34	2.96	0.37	17.9	158.07	3.88	0.152
Average	29.1	57.06	6.27	20.25	3.68	0.59	1.66	1.08	3.66	0.73	3.57	0.37	2.58	0.38	19.49	152.56	3.15	0.286

Table 4: Analytical Results of Trace Elements of Samples from the Early Cretaceous Intrusive Rocks

Sample No.	Trace Element Content (10^{-6})																			
	Rb	Pb	Zn	Cr	Ni	Co	W	Mo	Bi	Sr	Ba	Nb	Ta	Zr	Hf	Sn	Ag	Au	U	Th
PM002-1WL2	4.24	10.1	38.2	34.8	4.96	9.72	0.41	0.39	0.057	416	540	15.8	1.94	114	3.60	1.73	0.032	0.00108	1.0	12.2
PM002-1WL3	5.16	13.0	48.6	14.4	4.70	8.43	0.56	0.30	0.062	419	539	13.7	1.48	107	3.58	1.36	0.036	0.00108	1.3	12.0
PM002-2WLI	7.42	13.0	28.3	23.5	1.67	2.92	0.44	0.32	0.055	333	701	17.0	1.66	124	4.19	1.11	0.047	0.00054	2.2	13.9
PM002-4WL1	160	15.6	15.1	10.2	1.90	1.24	2.18	0.44	0.074	312	920	5.76	0.70	89.4	3.66	0.51	0.063	0.00151	1.5	15.4
PM003-2WL2	32.7	17.6	28.2	15.5	2.44	2.70	2.02	0.83	0.15	208	356	17.2	2.70	110	4.12	1.26	0.063	0.00211	2.5	42.0
PM003-5WL1	34.9	14.8	41.8	10.6	4.72	10.1	0.46	0.31	0.10	470	594	13.8	1.37	116	3.90	1.47	0.063	0.00155	1.76	11.1
ED306-WL1	7.44	17.8	28.0	18.4	6.5	4.22	1.46	1.00	0.18	497	780	9.32	0.84	104	4.10	3.12	0.079	0.0178	5.06	11.4
ED312-WL1	6.36	10.4	21.5	26.4	6.00	6.62	0.56	0.27	0.077	458	448	15.6	1.65	127	3.72	1.26	0.054	0.00234	2.18	14.0
ED315-WL1	7.68	14.1	38.8	12.8	3.97	6.50	0.57	1.04	0.074	524	554	11.8	1.08	135	4.31	1.70	0.050	0.00129	2.56	10.8
GD313-WL1	9.66	15.7	46.2	9.47	3.48	6.14	1.19	0.35	0.11	421	450	17.0	1.79	132	4.30	1.84	0.056	0.00106	2.46	12.7
HD229-WL1	10.7	17.1	43.2	22.0	9.43	8.90	3.00	1.31	0.18	450	569	16.3	1.64	136	4.14	3.41	0.051	0.019	2.74	18.3
Average	26.0	14.5	34.4	18.0	4.52	6.13	1.16	0.59	0.10	410	586	13.9	1.51	117	3.97	1.71	0.054	0.00449	2.53	15.8

Rare earth distribution curve show that Fig 6) the curve tilts to the right. Light rare earth is obvious of high fractionation. It belongs to earth enrichment type of light rare. Eu in local samples showed negative trough anomaly and loss. The heavy rare earth Gd-Lu element is nearly flat and the fractionation is unknown.

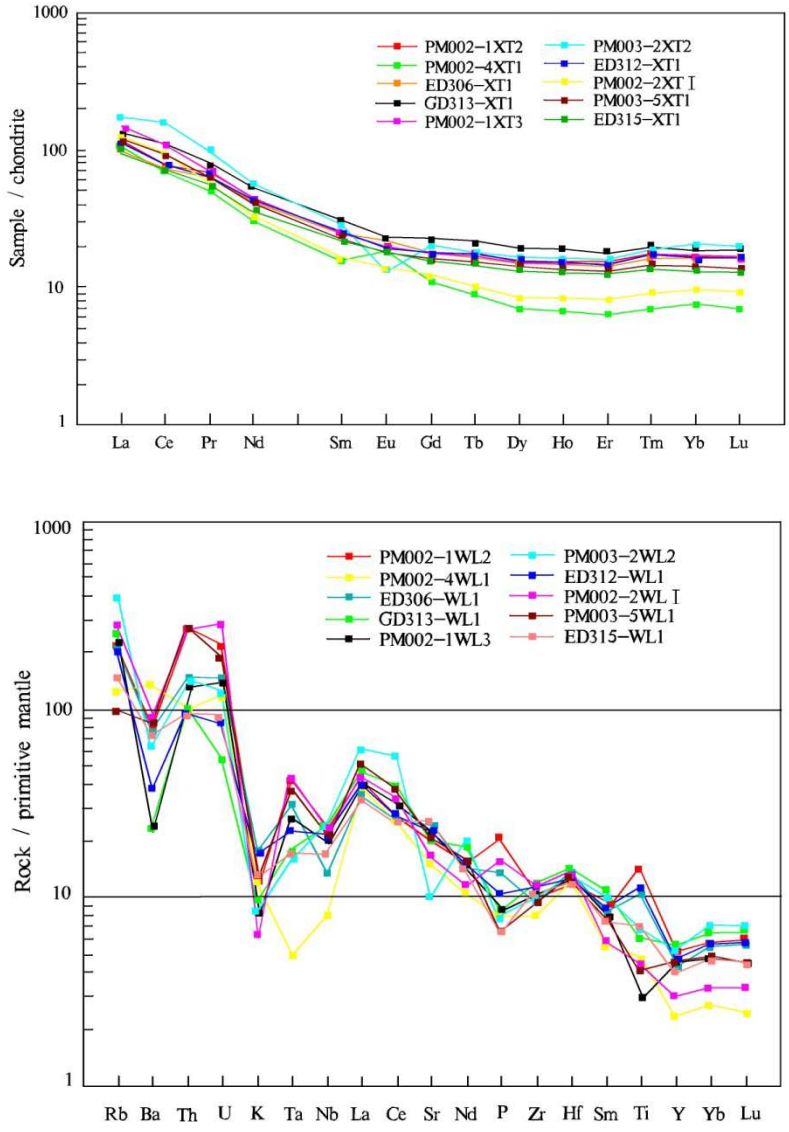

Figure 6: REE Distribution Patterns(a) and Spider Diagram of Trace Element Ratio (b) of Intrusive Rocks in the Study Area (from Sun and McDonough, 1989).

It reflected as moderately partial melting or strongly differentiated magmatic products (Wang et al., 2001). Large ion lithophile elements Rb, Sr are lower than diorite. The abundance of radioactive heating elements are also low.

The spider diagram of trace element ratio tilted to the right (Fig. 6), showing that Rb, Th, U and K of large ion incompatible elements (LILE) are significantly enriched The Nb, Ta and Ti of high field strength elements (HFSE) are significantly depleted. It indicates the characteristics of island arc magma (Wilson, 1989).

Zircon U-Pb Age

Zircons in granodiorite porphyry are pale yellow-colorless transparent. Zircon cathodoluminescence (CL) image show that(Fig 7) it is short columnar and high degree of self-shape, having typical magmatic shock ring, core mantle structure and grain between 100-200 μ m. In addition, residual crystals of gray-black columnar inherited zircons can be found in some zircons (Fig 7 b), which indicates that they are magmatic zircons (Bai et al., 2022).

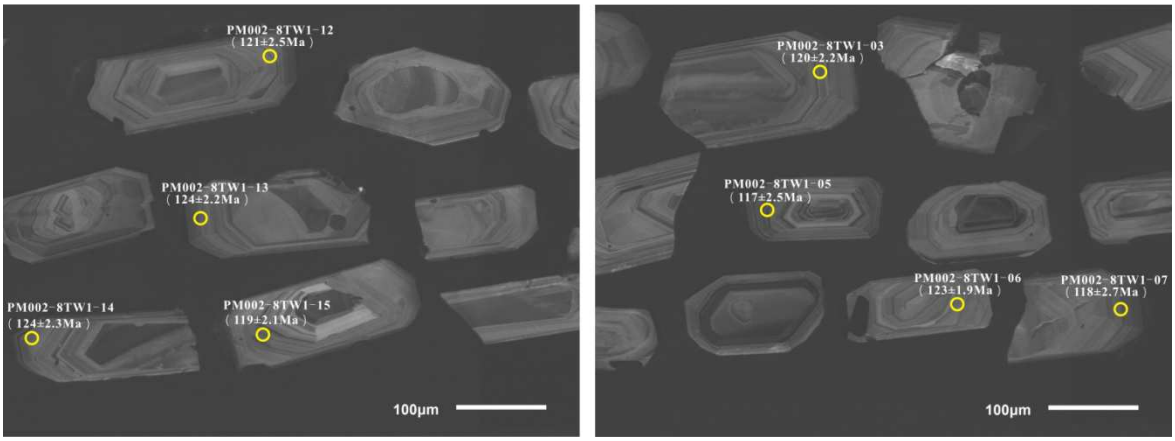

Figure 7: Cathodolumine Scence Images of Typical Single-Crystal Zircons from the Granodiorite Porphyry.

In zircon dating, granodiorite porphyry, medium-coarse biotite hornblende granodiorite and fine-grained biotite hornblende diorite respectly have 18， 17 and 11 measuring points. The U-Pb ages of the three types of rocks are shown in Table 5, Table 6 and Table 7.

Table 5 shows that the 206Pb / 238U age of granodiorite porphyry ranges from 117Ma to 124Ma. In the 206Pb / 238U-207Pb / 235U age harmonic diagram (Fig 8a), all data points are distributed on the harmonic line. The weighted average age is 120.33 ± 0.99Ma (Fig 8b). Therefore, 120Ma can be used as the crystallization age of granodiorite porphyry and its formation age is Early Cretaceous.

Table 5: LA-ICP-MS Analytical Results for the U-Pb Age Dating of Zircons from the Granodiorite Porphyry

Measuring Point	$\omega B/10^{-6}$			Th/U	Isotopic Ratio Corrected for Ordinary Lead						Isotopic Age Corrected for Common Lead /Ma					
	Pb	Th	U		$^{207}Pb/^{206}Pb$	±1σ	$^{207}Pb/^{235}U$	±1σ	$^{206}Pb/^{238}U$	±1σ	$^{207}Pb/^{206}Pb$	±1σ	$^{207}Pb/^{235}U$	±1σ	$^{206}Pb/^{238}U$	±1σ
PM002-8TW1-02	19.4	183	314	0.58	0.05513	0.00407	0.13948	0.00992	0.01880	0.00034	417	167	133	9	119	1.9
PM002-8TW1-03	21.2	217	303	0.72	0.04914	0.00337	0.12586	0.00840	0.01889	0.00036	154	156	120	8	120	2.2
PM002-8TW1-04	16.3	162	261	0.62	0.07168	0.00541	0.17621	0.01386	0.01826	0.00040	976	154	165	12	121	2.3
PM002-8TW1-05	27.1	262	433	0.61	0.05574	0.00335	0.14512	0.00823	0.01920	0.00031	443	133	138	7	117	2.5
PM002-8TW1-06	12.4	112	209	0.54	0.05122	0.00513	0.12631	0.01190	0.01846	0.00043	250	32	121	11	123	1.9
PM002-8TW1-07	18.7	186	319	0.58	0.05205	0.00358	0.13815	0.00944	0.01902	0.00033	287	157	131	8	118	2.7
PM002-8TW1-08	13.5	135	219	0.61	0.06144	0.00486	0.15865	0.01277	0.01881	0.00038	654	170	150	11	121	2.1
PM002-8TW1-10	25.1	225	323	0.70	0.05884	0.00738	0.14976	0.01647	0.01896	0.00037	561	276	142	15	120	2.4
PM002-8TW1-11	11.7	117	182	0.64	0.05826	0.00476	0.15091	0.01193	0.01887	0.00043	539	180	143	11	120	2.8
PM002-8TW1-12	14.8	131	239	0.55	0.07110	0.00495	0.18190	0.01230	0.01898	0.00039	961	144	170	11	121	2.5
PM002-8TW1-13	20.2	182	300	0.61	0.06483	0.00486	0.17641	0.01355	0.01943	0.00035	769	155	165	12	124	2.2
PM002-8TW1-14	21.1	201	308	0.65	0.05929	0.00518	0.14961	0.01119	0.01937	0.00037	589	195	142	10	124	2.3
PM002-8TW1-15	19.7	189	296	0.64	0.05080	0.00402	0.12992	0.00996	0.01858	0.00034	232	183	124	9	119	2.1
PM002-8TW1-16	17.6	175	297	0.59	0.06266	0.00516	0.15593	0.01228	0.01844	0.00035	698	178	147	11	118	2.2
PM002-8TW1-17	12.7	128	245	0.52	0.05537	0.00421	0.14344	0.01076	0.01882	0.00036	428	166	136	10	120	2.3
PM002-8TW1-18	16.4	150	250	0.60	0.05221	0.00472	0.12978	0.01139	0.01842	0.00038	295	207	124	10	118	2.4
PM002-8TW1-19	20.0	179	297	0.60	0.05103	0.00497	0.12623	0.01139	0.01894	0.00039	243	27	121	10	121	2.5
PM002-8TW1-20	14.4	143	261	0.55	0.04643	0.00471	0.11710	0.01123	0.01853	0.00034	20	235	112	10	118	2.1

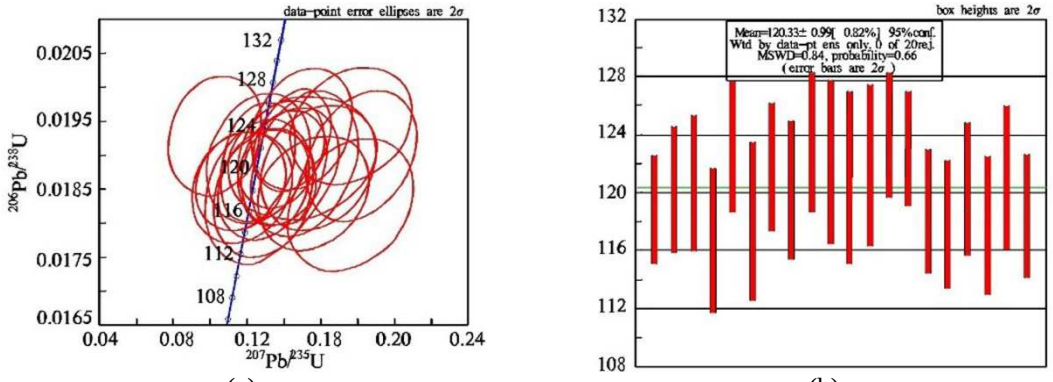

(a) (b)

Figure 8: The Concordant Diagram of LA-ICP-MS U-Pb Ages (a) and Histogram of Weighted Ages (b) of Zirconsfrom the Granodiorite Porphyry.

From Table 6, we can see that the 206Pb / 238U age of medium-grained biotite hornblende diorite is between 119Ma and 127Ma. In the 206Pb / 238U-207Pb / 235U age harmonic diagram (Fig 9a), all data points are distributed on the harmonic line. The weighted average is 122.5 ±2.0 (Fig 9b). Therefore, the crystallization age of medium-grained biotite hornblende granodiorite is 122.5 Ma.

Table 6: LA-ICP-MS Analytical Results for the U-Pb Age Dating of Zircons from the Medium Grained Granodiorite

Measuring Point	ωB/10⁻⁶				Isotopic Ratio Corrected for Ordinary Lead						Isotopic Age Corrected for Common Lead /Ma					
	Pb	Th	U	Th/U	$^{207}Pb/^{206}Pb$	±1σ	$^{207}Pb/^{235}U$	±1σ	$^{206}Pb/^{238}U$	±1σ	$^{207}Pb/^{206}Pb$	±1σ	$^{207}Pb/^{235}U$	±1σ	$^{206}Pb/^{238}U$	±1σ
PM002-1TW4-01	7.7	153	152	1.01	0.06817	0.00503	0.18097	0.01574	0.01922	0.00050	874	149	169	14	123	3.2
PM002-1TW4-02	8.4	126	202	0.63	0.05547	0.00349	0.14084	0.00978	0.01864	0.00045	432	141	134	9	119	2.8
PM002-1TW4-03	7.3	111	205	0.54	0.05276	0.00361	0.13652	0.00966	0.01920	0.00045	320	162	130	9	123	2.9
PM002-1TW4-04	8.1	116	228	0.51	0.05064	0.00344	0.13497	0.00937	0.01965	0.00062	233	157	129	8	125	3.9
PM002-1TW4-05	11.0	158	304	0.52	0.04821	0.00340	0.12615	0.00932	0.01968	0.00076	109	224	121	8	126	4.8
PM002-1TW4-06	8.4	123	243	0.51	0.05474	0.00310	0.13750	0.00787	0.01878	0.00051	467	95	131	7	120	3.3
PM002-1TW4-07	6.1	84	182	0.46	0.05952	0.00462	0.15226	0.01292	0.01908	0.00070	587	168	144	11	122	4.4
PM002-1TW4-08	7.5	103	214	0.48	0.05525	0.00357	0.13994	0.00918	0.01902	0.00053	433	144	133	8	121	3.3
PM002-1TW4-09	15.3	282	329	0.86	0.05126	0.00347	0.13522	0.00923	0.01963	0.00069	254	183	129	8	125	4.4
PM002-1TW4-10	4.2	56	141	0.40	0.07809	0.00697	0.19919	0.01706	0.01988	0.00098	1150	178	184	14	127	6.2
PM002-1TW4-11	12.2	180	345	0.52	0.04824	0.00398	0.12131	0.01002	0.01948	0.00131	122	172	116	9	124	8.3
PM002-1TW4-12	7.4	110	188	0.59	0.05743	0.00564	0.13607	0.01138	0.01928	0.00090	509	217	130	10	123	5.7
PM002-1TW4-13	5.9	77	149	0.52	0.06633	0.00517	0.17270	0.01347	0.01957	0.00072	817	158	162	12	125	4.5
PM002-1TW4-14	8.5	129	240	0.54	0.05914	0.00414	0.14841	0.01150	0.01900	0.00075	572	152	141	10	121	4.8
PM002-1TW4-15	9.0	120	284	0.42	0.04864	0.00475	0.12321	0.01345	0.01954	0.00117	132	215	118	12	125	7.4
PM002-1TW4-16	6.9	106	232	0.45	0.04716	0.00431	0.11696	0.01163	0.01979	0.00138	58	204	112	11	126	8.7
PM002-1TW4-17	7.9	106	230	0.46	0.05370	0.00521	0.14058	0.01531	0.01908	0.00113	367	220	134	14	122	7.2

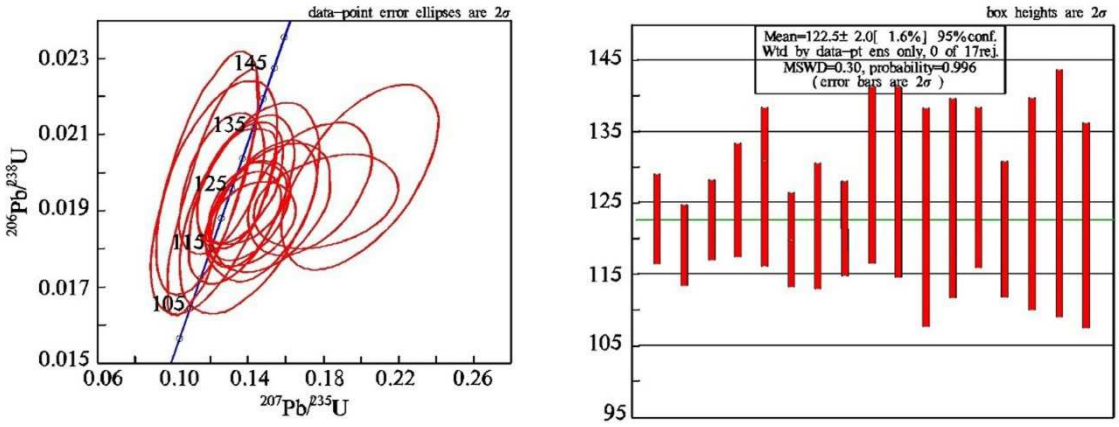

(a) (b)

Figure 9: The Concordant Diagram of LA-ICP-MS U-Pb Ages (a) and Histogram of Weighted Ages (b) of Zircons from the Medium Grained Granodiorite.

Similarly, from Table 7 and the 206Pb / 238U-207Pb / 235U age harmonic diagram of medium-fine biotite hornblende granodiorite (Fig. 10), its formation age is 125.7 Ma.

Table 7: LA-ICP-MS Analytical Results for the U-Pb Age Dating of Zircons from the Fine Grained Hornblende Biotite Granodiorite

Measuring Point	ωB/10⁻⁶			Th/U	Isotopic Ratio Corrected for Ordinary Lead						Isotopic Age Corrected for Common Lead /Ma					
	Pb	Th	U		$^{207}Pb/^{206}Pb$	±1σ	$^{207}Pb/^{235}U$	±1σ	$^{206}Pb/^{238}U$	±1σ	$^{207}Pb/^{206}Pb$	±1σ	$^{207}Pb/^{235}U$	±1σ	$^{206}Pb/^{238}U$	±1σ
PM002-10TW1-01	13.1	199	345	0.58	0.05230	0.00342	0.13779	0.00986	0.01937	0.00063	298	150	131	9	124	4.0
PM002-10TW1-02	11.6	172	301	0.57	0.04765	0.00304	0.12482	0.00856	0.01919	0.00050	83	150	119	8	123	3.1
PM002-10TW1-03	9.9	149	259	0.58	0.05509	0.00346	0.14193	0.00903	0.01892	0.00045	417	108	135	8	121	2.9
PM002-10TW1-04	6.1	57	148	0.39	0.08033	0.00700	0.21734	0.02146	0.01994	0.00099	1206	168	200	18	127	6.2
PM002-10TW1-05	11.4	162	335	0.48	0.04930	0.00309	0.13783	0.00985	0.02015	0.00045	161	146	131	9	129	2.9
PM002-10TW1-06	11.0	168	258	0.65	0.05706	0.00364	0.15522	0.01074	0.01967	0.00049	494	141	147	9	126	3.1
PM002-10TW1-07	14.1	219	358	0.61	0.05061	0.00290	0.13342	0.00879	0.02018	0.00080	233	131	127	8	129	5.0
PM002-10TW1-08	10.0	126	261	0.48	0.05936	0.00459	0.16365	0.01348	0.02048	0.00055	589	136	154	12	131	3.5
PM002-10TW1-09	9.2	139	250	0.56	0.04796	0.00355	0.12647	0.01007	0.02018	0.00087	98	167	121	9	129	5.5
PM002-10TW1-10	4.7	65	181	0.36	0.06096	0.01102	0.12188	0.01209	0.01964	0.00194	639	398	117	11	125	12.3
PM002-10TW1-11	8.7	132	230	0.57	0.07210	0.00666	0.18801	0.01621	0.01982	0.00074	989	189	175	14	127	4.6

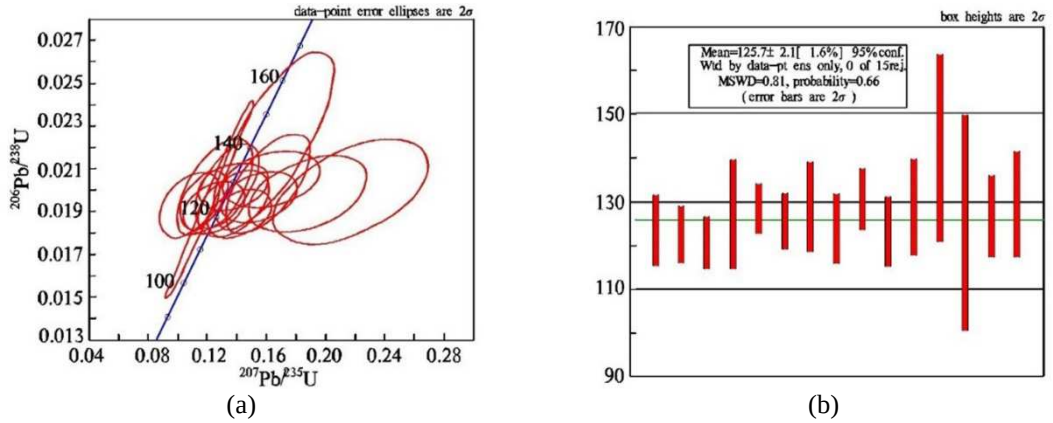

(a) (b)

Figure 10: The Concordant Diagram of LA-ICP-MS U-Pb ages (a) and Histogram of Weighted Ages (b) of Zircons from the Fine Grained Hornblende Biotite Granodiorite.

The above three groups of rock age data of granodiorite porphyry (120 Ma), medium-sized biotite hornblende granodiorite (122.5 Ma) and fine-sized biotite hornblende granodiorite (125.7 Ma) reflect that the emplacement age of Tuanjiedaban rock mass is Early Cretaceous.

Petrogenesis and Tectonic Environment

Magma Characteristic of Source Region

Incompatible elements have similar distribution coefficients which are not affected by the separation and crystallization. The mantle-derived materials only have minimal changes in the partial melting process. Therefore, they are often used to indicate the characteristics of the source region (Yang et al., 2021). The large-ion lithophile elements Rb, Th, U and K in Tuanjiedaban rock mass in the study area are obviously enriched. The highest value of Rb is 160×10^{-6}, and the average value is 26.02×10^{-6}. The high field strength elements Nb and Ta are obviously depleted. The distribution characteristics of these trace elements show that the study area has the characteristics of island arc magmatism (Wilson, 1989). On the discriminant diagrams of Rb- (Y + Nb), Nb-Y, Ta-Yb and Rb- (Yb + Ta) tectonic environment (Fig. 11) (Pearce et al.,1984; Taylor and McLennan, 1985), most samples fall in island-arc magmatic rock area. Only in the discrimination of Ta-Yb tectonic environment, two samples fall on the edge of island arc magma respectively, which may indicate that some magma formed from the melting of the crust in the late collision (Defant and Drummond, 1990).

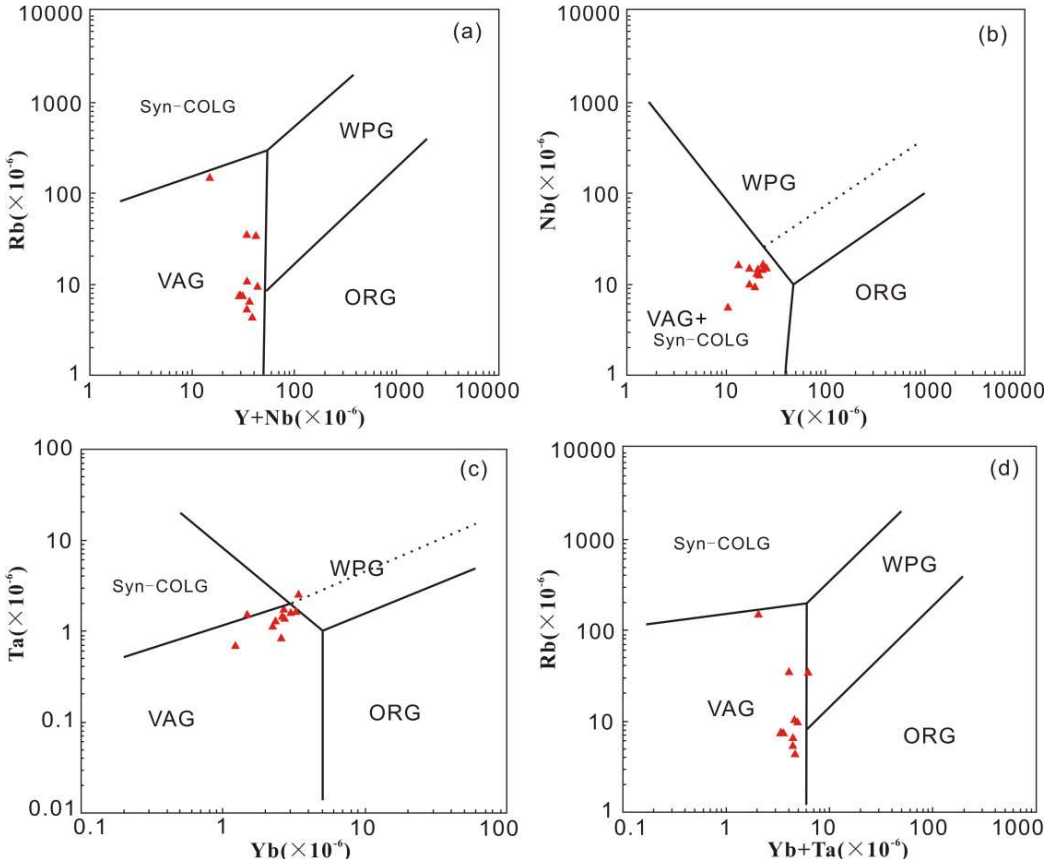

Figure 11: Rb-(Y+Nb) (Fig 11a), Nb-Y (Fig 11b), Ta-Yb (Fig 11c) and Rb-(Yb + Ta) (Fig 11d) Discriminant Diagrams for the Tuanjiedaban Intrusive (Syn-COLG: Syn-Collision Granites; WPG: within Plate Granites; ORG: Ocean Ridge Granites; VAG: Volcanic Arc Granites) (from the Pearce et al.,1984).

The Th / Ta ratios in granodiorites range from 6.29 to 22.0, much higher than the mantle ratio (1.1) (Palmf and O 'neill, 2014), indicating a clear genetic relationship between the rocks and the crust. The value indicates that the Rb / Sr ratio is small (the highest value is only one sample about 0.51).Most of which are between 0.01 and 0.07. The Eu of local samples shows negative trough anomaly, indicating that magma formation may be involved in mantle materials (Pearce et al., 1984; Wu et al.,1997). In addition, the dark-colored mineral inclusions in the intrusion also confirmed that a certain degree of crust-mantle contamination occurred during the magma formation (Du et al., 1993; Duan et al., 2013).

In summary, Tuanjiedaban intermediate-acid magmatic rocks have geochemical characteristics of arc volcanic rocks. The distribution patterns of trace elements and rare earths further confirm that the magma in this region has the characteristics of island-arc magma. The plate subduction leads to the addition of mantle-derived materials, and then crust-mantle contamination occurs (Song et al., 2019).

Petrogenesis

Petrochemical analysis of Tuanjieban rock mass shows that SiO2 is 57.56-72.35% (Table 1) with high potassium (K_2O content 2.88-7.05%) and Na_2O+K_2O content (content 5.7-10.41%). This high potassium and alkaline granite K_2O/Na_2O(0.97-3.53) is a typical type I granite (Green and Adam 2002; Thego et al., 2019), which corresponds to island arc type or post-collision granite. However, it may also inherit the environment from the above sources (Frost and Frost 2008). Apatite crystals and SiO_2 content in magma are not affected by oxygen fugacity and temperature, but inversely related (Tollari et al. 2006). The crystallization temperature of Tuanjieban rock mass is mainly between 800℃ and 950℃, which is the crystallization temperature condition of intermediate-acid magma. The content of P_2O_5 in middle rocks is relatively low and at the same level (Chappell 1999), which represents the strong crystallization differentiation of I-type granite (Chappell and White,2001). In the calc-alkaline tholeiite series, when P is supersaturated in magmatic hydrothermal solution, the increase of P_2O_5 content can only be caused by the increase of temperature (Tollari et al. 2006). Therefore, the SiO_2-P_2O_5 diagram indirectly shows that Tuanjiedaban pluton is not a single mantle-derived product of high-temperature melting and crystallization differentiation (Fig 12).

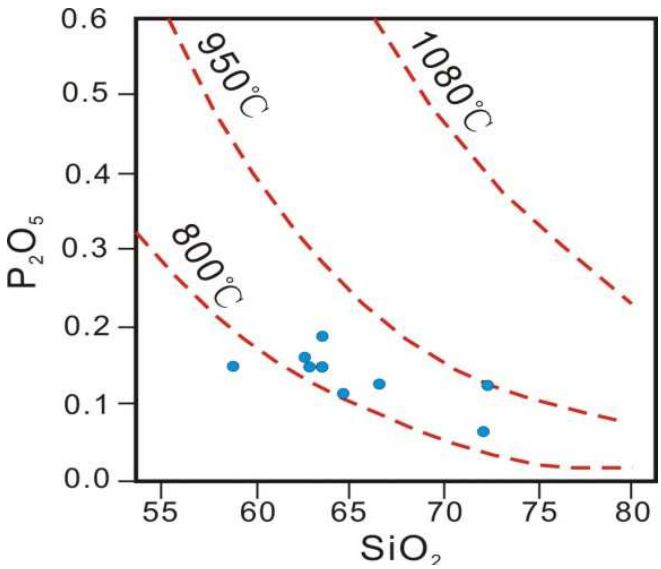

Figure 12: Diagrams of SiO_2-P_2O_5, The Red Dotted Line Indicatesisotherm of the P_2O_5,(from the Watson, 1982).

The contents of trace elements Cr, Ni, Co and Cu are high. It accessory minerals are apatite and zircon. The A/CNK value is mostly greater than 1.1 which belongs to peraluminous. The distribution curve of rare earth is right-angled and smooth with weaking Eu negative anomaly. It belongs to weak peraluminous calc-alkaline series and has obviously negative anomalies of trace elements Nb, Ta and Ti and positive correlation between Y and Rb content, all of which show that the characteristics of I-type granite (Chappell and White,2001;Li et al.,2006).

In the K_2O-Na_2O genetic discrimination diagram (Fig 13), most samples of Tuanjiedaban rock

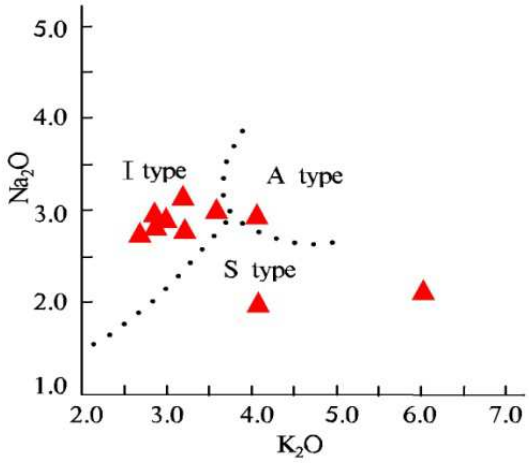

Figure 13: Genetic Discrimination Diagram of K_2O-Na_2O, (from the Collins et al., 1982).

Mass fall into I-type granite area. Some of them fall into S-type granite area. At present, many models have been proposed for the genesis of high-potassium calc-alkaline peraluminous I-type granite: partial melting of intermediate-basic crust (Roberts and Clemens, 1993), recrystallization or melting of high-potassium basalt (Sisson et al., 2005), partial melting of lower crust (Collins et al., 2016), the mixture of crustal melt and residual magma melt leads to isotope and trace element differentiation (Annen et al., 2006), the mixture of mantle and crustal components (Kemp et al., 2007), partial melting or recrystallization of neutral igneous rocks (Clemens et al., 2011；; Castro, 2013）. The A/CNK of the study area is 1.0-1.51, which shows the characteristics of high potassium felsic Al-saturated I-type granite (Zhu et al., 2020). The genetic characteristics of this kind of rock mass have been confirmed in Bangonghu-Nujiang suture zone (Wang et al., 2021; Li et al., 2016).

Tectonic Environment and Geological Significance

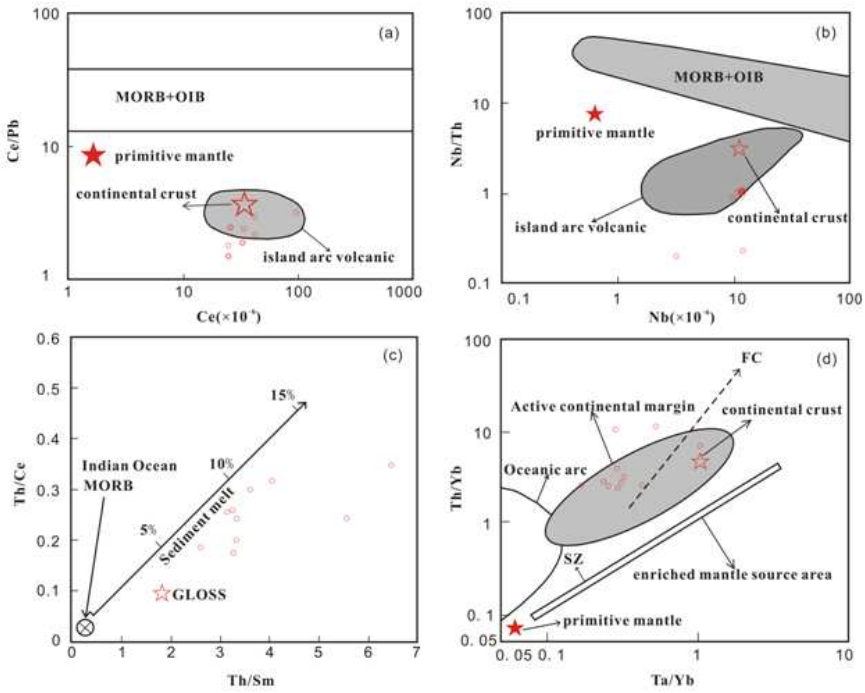

Figure 14: Ce/Pb-Ce (Fig 14a), Nb /Th-Nb (Fig 14b), Th /Ce-Th/Sm (Fig 14c) and Th/Yb-Ta/Yb (Fig 14d) Discriminant Diagrams of Tuandaban Island Arc Type Granite (a,b and d from Boztug et al.2007; Primitive Mantle from Hofman 1988; Continental Crust, MORB+OIB and Island Arc Volcanic Rock from Schmidberger and Henger 1999; c Shows the Arrow Line Marked with Sediment Melt in the Figure is the Mixing Line between Sediment Melt and Indian Ocean MORB Mantle, Indian Ocean MORB from Rehkamper and Hofmann 1997; GLOSS from Plank and Langmuir 1998; FC and SZ Respectively Represent Crystallization Separation and Subduction Zone in Fig 14d).

In the discrimination map of trace element tectonic environment (Fig 14), most of the samples fall in island arc volcanic areas (Fig. 14a, b),which shows that their magma source areas are consistent with island arc volcanic rocks, indicating that they are from the partial melting of mantle wedge in subduction zone. The A/ CNK value is mostly greater than 1.1, which belongs to peraluminous. It indicates that may be closely related to the crustal source and some samples fall on the periphery of the island arc volcano. On the Th /Ce-Th /Sm ratio diagram (Fig 14c), the tuanjiedaban rock mass is mostly distributed along the mixing line of the Indian Ocean MORB mantle and sediment melt, which indicates that the mantle source area is metasomatized by the sediment melt from subduction plate (Du et al., 1993) and the proportion of sediment melt in the source area of different rock masses is also different. The value indicates that there are two samples of subduction sediments (GLOSS, Fig 14c) in Tuanjiedaban, whose lithology is fine-grained hornblende granodiorite and granite porphyry (sample numbers are PM002-2WLI/ PM002-4WL1,Table 3, Table 4). Their Th contents respectively are 13.9×10-6 and 15.4×10-6 . The contents of Sm respectively are 2.51×10-6 and 2.38×10-6. Compared with the global average of trace elements in subduction sediments (Th-6.91, Sm-5.78)(Plank and Langmuir,1998), it shows the enrichment of Th and the loss of Sm.The value indicates that there are two samples of subduction sediments (GLOSS, Fig 14c) in Tuanjiedaban, whose lithology is fine-grained hornblende granodiorite and granite porphyry (sample numbers are PM002-2WLI/ PM002-4WL1,Table 3, Table 4). Their Th contents respectively are 13.9×10^{-6} and 15.4×10^{-6}. The contents of Sm respectively are 2.51×10-6 and 2.38×10-6. Compared with the global average of trace elements in subduction sediments

(Th-6.91, Sm-5.78) (Plank and Langmuir,1998), it shows the enrichment of Th and the loss of Sm. The above analysis shows that in Tuanjiedaban pluton, melting and contamination of part of the lower crust may result in magma crystallization differentiation (Collins et al., 2016). Th /Yb-Ta /Yb ratio diagram (Fig 14d) shows that these magma have the characteristics of continental margin arc. The crystallization separation is not obvious.

According to the zircon U-Pb age, the formation time of Tuanjiedaban pluton is 120-125.7Ma, while most people think that the age of Bangonghu Nujiang Tethys Ocean bidirectional subduction and the late Lhasa-Qiangtang plate collision is 130-110Ma (Li et al., 2011 ; ; Duan et al., 2013; Li et al.,2016 ; Zeng et al., 2020; Wang et al., 2021), which shows that the activity of Tuanjiedaban rock mass located in the northwest of Qiangtang Basin reflects the closing process of Tethys Ocean. Although there is still a big controversy about the closing time of Bangong Lake-Nujiang Tethys Ocean, the main controversy is the early Cretaceous ophiolite (～128Ma Jueweng ophiolite; Chen et al., 2006), Ocean Island (～116Ma Zhongcang Ocean Island and～132Ma Dongcuoyang Island; Fan et al.,2014; Wang et al.,2016), semi-deep sea sediments (～118Ma Zhaga Formation; Fan et al.,2015) and magmatic activities related to plate subduction (Wang et al.,2020; Pan et al., 2020). Another view is that the closing time of Bangonghu Nujiang Tethys Ocean is from Late Jurassic to Early Cretaceous, and its evidence is regional stratigraphic contact relationship, change of sedimentary facies, anatexic granite and etc. (Kapp et al.,2007; Ma et al.,2017）.

The continental complex of the first member of Abushan Formation (K2a1) of Late Cretaceous distributed in the study area, such as conglomerate and calcareous fine sandstone. It proves that the ocean basin was closed in this period and entered the stage of intercontinental evolution. This feature is also confirmed regionally (Wu et al.,2019). The continuous north-south collision and compression can lead to crust thickening and local melting (Guynn et al., 2006;Song et al., 2019 ; Zhao et al.,2019). Granitic magmatic rocks in Tuanjieban restricted the evolution of Bangonghu-Nujiang suture zone in Cretaceous. In the middle and late Early Cretaceous, the Bangonghu Nujiang Tethys Ocean subducted, reduced, collided and closed to the north. The ocean crust lithosphere is sank, causing the underplating of mantle-derived magma, accompanied by the melting of some crust. Therefore, the tuanjie Daban magma activity was 120-125.7Ma. It revealed the closing process of Tethys Ocean and the north-south plate compression process.

CONCLUSIONS

- The Tuanjie Daban rock mass is mainly composed of deep-formed intermediate-acid intrusive bodies and a small amount of hypabyssal porphyry. The rock mass is produced by stock, dikes and etc. It has fine-medium grain structure, spot structure and block structure. This kind of rock mass are unconformably covered by the angle of the first member of the Abushan Formation (K2a1) in Late Cretaceous.
- Petrogeochemical analysis shows that this set of intermediate-acid intrusive rocks has high silicon, aluminum and alkaline. The content of A / CNK is more than 1.1, belonging to calc-alkaline series rocks. Trace elements of Rb, Th, U and K are significantly enriched. The Nb, Ta and Ti are significantly depleted. Heavy rare earth is obvious of fractionation. Light rare earth is enriched. Eu is anomaly negative valley. The above show that the rock mass has island arc magmatic characteristics.

- Zircon U-Pb dating shows that the activity time of the rock mass is 120-125.7 Ma, which belongs to the middle and late Early Cretaceous. The magma source area is characterized by arc volcanic rocks, belonging to high potassium calc-alkaline per aluminous I-type granite. The Bangonghu Nujiang Tethys Ocean sub ducted and collided northward. The subsidence of oceanic lithosphere caused the under plating of mantle-derived magma. At the same time, the melting of partial crust led to the formation of magma.

ACKNOWLEDGMENTS

This project was funded by the China Geological Survey (No.1212011221094) and the Projects of Talents Recruitment of GDUPT (520130).

REFERENCES

1. *Andersen T.,2002. Correction of common lead in U-Pb analyses that do not report 204Pb. Chemical Geology, 192,59-79.*
2. *Annen C, Blundy J D, Sparks R S J, 2006. The genesis of intermediate and silicicmagmas in deep crustal hot zones.Journal of Petrology, 47, 505-539.*
3. *Bai R L,Hu J R, Zhao F F,Yu Z Y,Wang X M,Wang L X,Chen X F,Yang Y J,Zhou H L,Guo D B,2021. Zircon U-Pb Ages and Hf Isotopic Characteristics and Their Geological Significances of Syenogranite in the Shuangjianshan Gold Deposit in the Beishan Orogenic Belt, Gansu Province. Bulletin of Mineralogy, Petrology and Geochemistry,40,https://doi.org/10.19658/j.issn.1007-2802.2021.40.113*
4. *Boztug D, Harlavan Y and Arehart G B.2007.K-Ar age, whole-rock and isotope geochemistry of A-type granitoids in the Diverigi-Sivas Region, eastern-central Anatolia, Turkey. Lithos,97,193-218.*
5. *Castro A, 2013.Tonalite-granodiorite suites as cotectic systems: a review ofexperimental studies with applications to granite (sensulato) petrogenesis. Earth-Science Reviews, 124,68-95.*
6. *Chappell B W, White A J R. 2001.Two contrasting granite types: 25 years later.Australian Journal of Earth Sciences,48:489-499.*
7. *Chappell B W, 1999. Aluminium saturation in I- and S-type granites and the characterization of fractionated haplogranites. Lithos, 46:535-551.*
8. *Che X,Liu Y M,Fan J J, Yu Y P, Guo R H, Quan L C, Xie C M, Wang M. 2021. Late Cretaceous Dongco granodiorite porphyry, Tibet: Product of lithospheric delamination. Geological Bulletin of China, 40(8) :1357-1368*
9. *Chen Y L, Zhang K Z, Yang Z M, Luo T, 2006. Discovery of a complete ophiolite section in the Jueweng area, Nagqu County, in the central segment of the Banggong Co-Nujiang zone, Qinghai-Tibet Plateau. Geological Bulletin of China, 25(6):694-699.*
10. *Clemens J D, Stevens G, Farina F, 2011.The enigmatic sources of I-type granites: the peritectic connexion,Lithos,126,174-181.*

11. *Collins W J, Beams S D, White A J R, Chappell B W,1982.Nature and Origin of A-Type Granites with Particular Reference to Southeastern Australia. Contributions to Mineralogy and Petrology, 80:189-200.*
12. *Collins W J, Huang H Q, Jiang X Y, 2016. Water-fluxed crustal melting produces Cordilleran batholiths. Geology, 44, 143-146.*
13. *Defant M J, Drummond M S, 1990. Derivation of some modern arc magmas by melting of young subducted lithosphere, Nature, 347,662-665.*
14. *Du D D, Qu X M, Wang G H, Xin H B and Liu Z B. 2011. Bidirectional subduction of the Middle Tethys oceanic basin in the west segment of Bangonghu-Nujiang suture，Tibet: Evidence from zircon U-Pb LAICPMS dating and petrogeochemistry of arc granites. Acta Petrologica Sinica, 27(7):1993-2002.*
15. *Duan H R, Kang MZ, Wu SY, Chen LK, Jiao JS,2020. Uplife rate of the Tibetan Plateau constrained by GRACE time-variable gravity field. Chinese Journal of Geophysics, 63(12),4345-4360.*
16. *Duan Z M，Li G M，Zhang H，Li Y X,Duan Y Y, 2013.Zircon U-Pb Age & Geochemical Characteristics of theQuartz Monzobiorite and Metallogenic Background of the SenaGold Deposit in Duolong Metallogenic Concentrated Area, Tibet. Journal of Jilin University(Earth Science Edition), 43(6):1864-1877.*
17. *Fan J J,2016. Reconstructing the late Mesozoic closing process of the middle andwestern segments of the Bangong-Nujiang Ocean in space and time. Jilin University,1-174.*
18. *Fan J J, Li C, Liu Y M, Xu J X, 2015. Age and nature of the Late Early Cretaceous Zhaga Formation, northern Tibet: Constraints on when the Bangong-Nujiang Neo-Tethys ocean closed, International Geology Review, 57(3),342-353.*
19. *Fan J J, Li C, Xie C M, Wang M, 2014. Petrology, geochemistry, and geochronology of the Zhonggang ocean island, northern Tibet: implications for the evolution of the Banggongco–Nujiang oceanic arm of the Neo-Tethys, International Geology Review,56,1504–1520. https://doi:10.1080/00206814.2014.947639*
20. *Frost B R, Frost C D, 2008. A geochemical classification for feldspathicigneous rocks, Journal of Petrology, 49(11):1955-1969.*
21. *Geng Q R, Mao X C, Zheng Z, Peng Z M, Guan J L, 2015. New Understanding in the Middle and West Part of Bangong Lake-Nujiang River Metallogenic Belt and Its lmplication for Prospecting. Geological Survey of China, 2(2):1-11.*
22. *Green T H, Adam J, 2002. Pressure effect on Ti- or P-rich accessorymineral saturation in evolved granitic melts with differing K2O/Na2O ratios, Lithos, 61,271-282.*
23. *Guynn J H, Kapp P, Pullen A, Heizler M, Gehrels G, Ding L,2006.Tibetan basement rocks near Amdo reveal "missing" Mesozoic tectonism along the Bangong suture, central Tibet, Geology, 34(6),505-508. https://doi:10.1130/g22453.1*
24. *Hofmann A W, 1988. Chemical differentiation of the Earth: The relationship between mantle，continental crust and oceanic crust. Earth and Planetary Science Letters, 90,297-314.*

25. *Huang J J,2001.Structural Characteristics of the Basement of the Qiangtang Basin, Acta Geologica Sinica 75(3):333-337.*
26. *Kapp P，De Celles P G，Gehrels G E，Heizier M, Ding L, 2007.Geological records of the Lhasa-Qiangtang and Indo-Asian collisionsin the Nima area of central Tibet,Geological Society of AmericaBulletin, 119(7),917-932.*
27. *Kemp A I, Hawkesworth C J, Foster G L, Paterson B A, Woodhead J D, Hergt, J M, Gray C M, Whitehouse M J,2007. Magmatic and crustal differentiation history of granitic rocks from Hf-O isotopes in zircon,Science,315,980-983.*
28. *Li G M, Duan Z M, Liu B, Zhang H, Dong S， Zhang L, 2011.The discovery of Jurassic accretionary complexes in Duolong area, northern Bangong Co-Nujiang suture zone, Tibet，and its geologic significance. Geological Bulletin of China, 30 (8):1256-1260.*
29. *Li J X, QinK Z, Li G M, Xiao B, Zhao J X, Cao M J, Chen L,2013.Petrogenesis of ore-bearing porphyries from the Duolong porphyry Cu-Au deposit, central Tibet: Evidence from U-Pb geochronology, petrochemistry and Sr-Nd-Hf-O isotope characteristics,Lithos,160(1),216-227.https://doi:10.1016/j.lithos.2012.12.015*
30. *Li S M,Zhu D C, Wang Q, Zhao Z D, Sui Q L, Liu S A, Liu D, Mo X X, 2014.Northward subduction of Bangong–Nujiang Tethys: Insight from Late Jurassic intrusive rocks from Bangong Tso in western Tibet, Lithos, 205,284-297.*
31. *Li X H, Li Z X, Sinclair J A, Li W X, Carter G, 2006. Revisiting the "Yanbian Terrane" : Implications for Neoproterozoic tectonic evolution of the western Yangtze Block, South China, Precambrian Research,151,14-30.*
32. *Li X K, Li C, Sun Z M, Wang M, 2016. Origin and tectonic setting of the giant Duolong Cu-Au deposit, South Qiangtang Terrane, Tibet: Evidence from geochronology and geochemistry of Early Cretaceous intrusive rocks, Ore Geology Reviews,80,61-78. https://doi:10.1016/j.oregeorev.2016.06.025*
33. *Liang X, Wang G H, Yang B, Ran H, Zheng Y L, Du J X, Li L G, 2017.Stepwise exhumation of the Triassic Lanling high-pressure metamorphic belt in Central Qiangtang, Tibet: insights from a coupled study of metamorphism, deformation, and geochronology, Tectonics, 36(4), 652-670.*
34. *Liu Y M, Li C, Li S Z, Xie C M, Wang M, Fan J J, Liu J H, Guo R H, 2018.The Early Cretaceous Duguer metagabbro from Qiangnan-Baoshan block, Tibet Plateau: Implications for the subduction and closure of Bangong Co-Nujiang Ocean. Geological Bulletin of China, 37(8):1450-1463.*
35. *Liu Y S, Gao S,Hu Z C, Gao C G, Zong K Q, Wang D B, 2010. Continental and Oceanic Crust Recycling-induced Melt–Peridotite Interactions in the Trans-North China Orogen: U-Pb Dating, Hf Isotopes and Trace Elements in Zircons from Mantle Xenoliths, Journal of Petrology, 51,537-571.*
36. *Luo L Q, Zhan X C, Li G H,2008. X-ray fluorescence spectrometer. Beijign: Chemical Industry Press,1-188.*

37. *Ma A L，Hu X M，Garzanti E，Han Z, Lai W, 2017.Sedimentary andtectonic evolution of the southern Qiangtang basin: Implications forthe Lhasa-Qiangtang collision timing, Journal of Geophysical Research: Solid Earth, 122(7),4790-4813.*
38. *Palmf H, O'neill H S C, 2014. Cosmochemical estimates of mantle composition, Treatise on Geochemistry (Second Edition) ,3,1-39.*
39. *Pan G T，Wang L Q，Geng Q R，Yin F G，Wang B D，Wang D B，PengZ M，Ren F, 2020. Space-time structure of the Bangonghu-shuanghu-Nujiang-Changning-Menglian Mega-uture zone: A discussion on geology and evolution of the Tethys Ocean. Sedimentary Geology and Tethyan Geology, 40(3):1-19.*
40. *Papu D M, Philip M P, 1989.Tectonic discrimination of granitoids. Geological Society of America Bulletin,101: 635-643.*
41. *Pearce J A, Harris N B W, Tigdle A G, 1984.Trace element discrimination diagram for the tectonic interpretation of graniticrocks, Journal of Petrology, 25(4):956-983.*
42. *Peccerillo A, TaylorS R, 1976. Geochemistry of Eocene calcalkaline volcanic rocks from the Kastamonu area, Northern Turkey.ContributionstoMineralogyandPetrology,58:63-81.*
43. *Plank T, Langmuir C H, 1998. The chemical composition of subducting sediment and its consequences for the crust and mantle, Chemical Geology, 145,325-394.*
44. *Rehkamper M, Hofmann A M, 1997.Recycled ocean crust and sediment in Indian Ocean MORB. Earth and Planetary SciencesLetters,147,93-106.*
45. *Roberts M P, Clemens J D, 1993.Origin of high-potassium, calc-alkaline, I-typegranitoids, Geology, 21, 825-828.*
46. *Schmidberger S S, Henger E, 1999. Geochemistry and isotope systematic of calc-alkaline volcanic rocks from the Saar-Nahe basin(SW Germany):Implications for Late-Variscan orogenic development. Contributions to Mineralogy and Petrology,135,373-385*
47. *Shi J,2013. Determination of Trace Ag in the Samples of Rooks, Soils,Stream Sediments by ICP-MS. Contemporary Chemical Industry, 42(4):526-528.*
48. *Sisson T W, Ratajeski K, Hankins W B, Glazner A F, 2005.Voluminousgraniticmagmas from common basaltic sources, Contributions to Mineralogy and Petrology, 148, 635-661.*
49. *Song Y，Zeng Q G，Liu H Y，Liu Z B，Li H F and Dexi Y Z.2019.An innovative perspective for the evolution of Bangong- Nujiang Ocean: Also discussing the Paleo- and Neo-Tethys conversion. Acta Petrologica Sinica, 35(3):625-641*
50. *Sun J, Mao J W, Beaudoin G, Duan X Z, Yao F J,Ouyang H G, Wu Y, Li Y B, Meng X Y, 2017.Geochronology and geochemistry of porphyritic intrusions in the Duolong porphyry and epithermal Cu-Au district, central Tibet: Implications for the genesis and exploration of porphyry copper deposits, Ore Geology Reviews,80: 1004-1019.https://doi.org/10.1016/j.oregeorev.2016.08.029.*

51. *SunS, McDonoughWF.,1989. Chemical and isotopic systematics of oceanic basalts: implications for mantle composition and processes. Geological Society, London, Special Publications, 42(1):313- 345.*
52. *Taylor S R, McLennan S M, 1985. The continental crust: Its composition and evolution. Oxford: Blackwell Scientific Publication, 1-132.*
53. *Tepper J H, Nelson B K, Bergantz G W, 1993.Petrology of the Chilliwackbatholith, North Cascades, Washington: Generation of calc-alkalinegranitoids by melting of mafic lower crust with variable water fugacity, Contributions to Mineralogy and Petrology,113,333-351*
54. *Thyego R S, Valderez P F, Mariucha Maria C L, Alcides N S,2019.Geochemical and isotope evidence for mantle ‐derived source rockof high ‐K calc ‐alkaline I ‐type granites, Pernambuco-Alagoas Domain, northeastern Brazil, International Journal of Earth Sciences, 108,1095-1120.*
55. *Tollari N, Toplis M J, Barnes S J, 2006. Predicting phosphate saturationin silicate magmas: an experimental study of the effects ofmelt composition and temperature, Geochimica et Cosmochimica Acta, ,70(6),1518-1536*
56. *Wang B D, Wang L Q, Chung S L, Chen J L, Yin F G, Liu H, Li X B, Chen L.K, 2016. Evolution of the Bangong–Nujiang Tethyan ocean: Insights from the geochronology and geochemistry of mafic rocks within ophiolites,.Lithos, 245, 18-33.https:// doi:10.1016/j.lithos.2015.07.016*
57. *Wang D B，Tang Y，Luo L，Liao S Y，Yin F G and Wang B D, 2017.Late Oligocene crustal anatexis and melt/fluid migration in the Ailao Shan tectonic belt: Evidences from zircon U-Pb ages and trace element compositions. Acta Petrologica Sinica,(7):2037-2053.*
58. *Wang Q，Xu J F，Zhao Z H，Wang R J，Qiu J X and Bao ZW. 2001. The petrogeaesis and geodynamic significances of HREE depleted granitoids duriag Yanshan period in the Dahie Mountains. Acta Petrologica Sinica, 17(4):551-564.*
59. *Wang W, Wang M.Zhai Q G，Xie C M，Hu P Y，Li C，Liu J H, LuoA B, 2020.Transition from oceanic subduction to continental collision recorded in the Bangong-Nujiang suture zone: Insights from Early Cretaceous magmatic rocks in the north-central Tibet, Gondwana Research, 78, 77-91.*
60. *Wang W，Zhai Q G，Hu P Y，Tang Y，Zhu Z C and Wu H. 2021. Cretaceous magmatic rocks in the Nyima area，North Tibet: Constraints for the tectonic evolution of the Bangong-Nujiang suture zone. Acta Petrologica Sinica, 37(2) : 545-562.*
61. *Watson E Bruce,1979. Apatite saturation in basic to intermediate magmas. Geophysical Research Letters, 6(12), 937–940.*
62. *Wilson M, 1989. Igneous Petrogenesis, London: Unwin Hyman, 1-486.*
63. *Wu F Y, Jiang B M, Lin Q, 1997. Isotopic characteristics and crustal growth significance of post orogenic granites in the northern orogenic belt of China, Chinese Science Bulletin, 42(20):2188-2192.*
64. *Wu H, Chen J W, Wang Q, Yu Y P, 2019.Spatial and temporal variations in the geochemistry of Cretaceous high-Sr /Y rocks in Central Tibet, American Journal of Science,319(2),105-121.*

65. *Wu Y, Chen S Y, Qin M K, Guo D F, Guo G L, Zhang C, Yang J S, 2018. Zircon U-Pb Ales of Dongcuo Ophiolite in Western Bangonghu-Nujiang Suture Zone and Their Geological Significance. Earth Science,43(4) :1070-1084.*

66. *Yang H W, Wei L Y, Wang J Z, Li G Y, Zhang X K, Zhang Z, Tian C, Kou S L, Sun X,2021.A Study of Zircon U-Pb Ages and Geochemical Characteristics of the Gengzhaxi Granodiorite in the Western Qinling Orogen. Bulletin of Mineralogy, Petrology and Geochemistry,40,https://doi.org/10.19658/j.issn.1007-2802.2021.40.084*

67. *Zeng Q G,Wang B D, Xiluo LJ, Mao G Z, Liu H Y, Liu G X, 2020. Suture Zones in Tibetan and Tethys Evolution，Earth Science. 45(8):2735-2763.*

68. *Zeng Y C，Xu J F，Chen J L, Wang B D, Kang Z Q, 2018.Geochronological and geochemical constraints on the origin of the Yunzhug ophiolite in the Shiquanhe-Yunzhug-Namu Tso ophiolitebelt，Lhasa Terrane,Tibetan Plateau. Lithos，300-301:250-260.*

69. *Zhao S R, Ciwang R Z, La B, 2015.Five regional geological and mineral survey reports in maierze area, Gaize County, Tibet (1:50000),Geological Survey Institute of Tibet Autonomous Region,1-129.*

70. *Zhao Z B, Bons P D, Wang G,Soesoo A, Liu Y,2015.Tectonic evolution and high pressure rock exhumation in the Qiangtangterrane, central Tibet, Solid Earth, 6(2),457- 473.*

71. *Zhao Z B, Bons P D, Li C, Wang G H, Ma X X, Li G W, 2019.The Cretaceous crustal shortening and thickening of the South Qiangtang Terrane and implications for proto-Tibetan Plateau formation,Gondwana Research,78,141-155.https://doi:10.1016/j.gr.2019.09.003*

72. *Zheng H T, Zheng Y Y, Xu J, Wu S, Guo J C, Gao S B, Ci Q,2018.Zircon U-Pb Ages and Petrogenesis of Ore-Bearing Porphyry forQingcaoshan Porphyry Cu-Au Deposit, Tibet. Earth Science, 43(8):2858-2874.*

73. *Zhou J S, Meng X J, Zang W S, Yang Z S, Xu Y T and Zhang X. 2013. Zircon U-Pb geochronology and trace element geochemistry of the ore-bearing porphyry in Qingcaoshan porphyry Cu-Au deposit, Tibet and its geological significance. Acta Petrologica Sinica,29(11):3755-3766*

74. *Zhu R Z, Lai S C, Qin J F, Santosh M, Zhao S W, Zhang E C, Zong C L, Zhang X L, Xue Y Z, 2020.Genesis of high-potassium calc-alkaline peraluminous I-type granite: New insights from the Gaoligong belt granites in southeastern Tibet Plateau, Lithos, 105343. https://doi:10.1016/j.lithos.2019.105343*

75. *Zhu X P, Chen H A, Liu H F, Ma D F，Li G M, Huang H X，Zhang H, Liu C Q，Wei L J, 2015. Zircon U-Pb Ages，Geochemistry of the Porphyries from the Duobuza Porphyry Cu-Au Deposit，Tibet and Their Metallogenic Significance. Acta GeologicaSinica, 89(3):534-548.*